Holocene constraints on simulated tropical Pacific dynamics

J. Emile-Geay[1*], K.M. Cobb[2], M. Carré[3], P. Braconnot[4], J. Leloup[5], Y. Zhou[1],

S.P. Harrison[6], T. Corrège[7], M. Collins[8], R. Driscoll[9], M. Elliot[10],

H.V. McGregor[11], B. Schneider[12], A. Tudhope[9]

[1]*Department of Earth Sciences, University of Southern California, Los Angeles, CA 90089, USA*

[2]*School of Earth and Atmospheric Sciences, Georgia Institute of Technology, Atlanta, GA 30332, USA*

[3]*UM2-CNRS-IRD, Institut des Sciences de l'Evolution, Université Montpellier 2, Montpellier 34095, France*

[4]*IPSL/LSCE, unité mixte CEA-CNRS-UVSQ, Gif sur Yvette 91191, France*

[5]*Sorbonne Universités, UPMC Univ. Paris 6, LOCEAN/IPSL, UMR 7159, CNRS-IRD-MNHN, Paris, France*

[6]*Centre for Past Climate Change and School of Archaeology, Geography and Environmental Sciences (SAGES) University of Reading, Whiteknights, Reading, RG6 6AB, UK*

[7]*UMR 5805 EPOC, Université de Bordeaux, Pessac, France*

[8]*College of Engineering, Mathematics and Physical Sciences, University of Exeter, Laver Building, North Park Road, Exeter, EX4 4QE, UK*

[9]*University of Edinburgh, School of GeoSciences, James Hutton Road, Edinburgh EH9 3FE, UK*

[10]*Paleoclimats Paleoenvironnements Bioindicateurs, Université de Nantes, LPGNantes, 2 rue de la Houssinière, Nantes 44300, France*

[11] *School of Earth and Environmental Sciences, University of Wollongong, Wollongong, NSW, Australia*

[12] *Institut für Geowissenschaften, Universität Kiel, D-24118 Kiel, Germany*

The El Niño-Southern Oscillation (ENSO) influences climate and weather over much of the globe, so uncertainties in its response to external forcing[1] hinder long-range climate predictability. Modeling studies have argued that such forcings may affect ENSO either via the seasonal cycle[2–6] or extratropical influences[7–9], but this link is poorly constrained by the short instrumental record. Here we synthesize a pan-Pacific network of high-resolution marine biocarbonates spanning discrete snapshots of the Holocene (past $\sim$ 10,000 years), which we use to constrain a set of global climate model (GCM) simulations via a forward model[10] and a consistent treatment of uncertainty. Observations suggest important reductions in ENSO variability throughout the interval, most consistently during 3-5 kyBP, when $\sim$2/3 reductions are inferred. The magnitude and timing of these ENSO variance reductions bear little resemblance to those simulated by GCMs, or to equatorial insolation. The central Pacific witnessed a notable mid-Holocene increase in seasonality, at odds with the reductions[11] simulated by GCMs. Finally, while GCM aggregate behavior is consistent with an inverse relationship between seasonal amplitude and ENSO-band variance in sea-surface temperature[3,6,12,13], this relationship is not borne out by these observations. The synthesis suggests that tropical Pacific climate is highly variable, but exhibited millennia-long periods of reduced ENSO variability whose origins, whether forced or unforced, are a crucial issue for model development and long-term climate prediction.

ENSO, the non-linear interaction between the tropical Pacific atmosphere and ocean, is the leading pattern of global interannual variability, with important physical, ecological, and human impacts. Yet, predicting its long-term behavior in the face of continued greenhouse forcing has proven elusive[1]. While the predictive skill of climate models at interannual timescales can be tested using instrumental observations, such records are too short to evaluate the fidelity of model-simulated tropical Pacific variability on decadal- to centennial-timescales, i.e. those relevant for future climate projections. This motivates the use of paleoclimate observations, which cover a much longer time span and predate the observations used to develop and tune climate models, hence providing an out-of-sample test of their predictive ability[14].

The mid-Holocene (MH, ca 6,000 yrs before present; 6 kyBP) represents a key target for evaluating the simulated response of ENSO to changes in external forcing. While ice volume and greenhouse gas concentrations were essentially similar to today, the latitudinal and seasonal distribution of incoming solar radiation (insolation) was markedly different as a result of precession[15]: seasonal contrast was amplified in the northern hemisphere and reduced in the southern hemisphere. Thus, the mid-Holocene provides an opportunity to explore the link between changes in the seasonal cycle, meridional asymmetry in the equatorial zone, and ENSO behavior. Several paleoclimate records from the circum-Pacific region have been interpreted as showing that ENSO was markedly weaker during the MH [16–18]. Various models have also simulated a weaker ENSO during this period[2,4,5,8,11]. This MH reduction in ENSO activity has been dynamically linked to an insolation-driven increase in the amplitude of the annual cycle (AC) in near-equatorial SST[4,5,11], in line with evidence for a negative correlation between ENSO and the AC documented in instrumen-

tal observations[19] and modeling studies of both current and past climate states[2,6,12,13,20]. Several mechanisms have been proposed to account for the seasonal cycle influence on ENSO: frequency locking[3,12]; nonlinear resonance between annual and internal modes[21,22], and combination tones of ENSO and the AC[23]. We note, however, that the inverse link between ENSO variance and AC amplitude is not universal amongst models[4,15]. While some seasonally-resolved paleoclimate records suggest a strong dynamical link between precessional forcing and ENSO activity[24], reconstructions of central and eastern Pacific ENSO variance do not show such trends[25,26]. A synthesis of the available paleoclimate observations and paleoclimate models simulations of ENSO and the annual cycle is timely, and would help to address the question of whether most, if not all, of the low-frequency modulation of ENSO variability is endogenous[27].

Here we synthesize high-resolution, well-dated paleoclimate records from across the tropical Pacific to constrain the sensitivity of the tropical Pacific climate system to orbital forcing through the Holocene. We compare these data to an ensemble of nine state-of-the-art global climate models (GCMs) from the Paleoclimate Modeling Intercomparison Project (PMIP3[28]), which include simulations of pre-industrial (*piControl*) as well as industrial era (*historical*) and MH (*midHolocene*) climate (Table S2). The datasets represent the most comprehensive collection of oxygen isotope measurements on Holocene corals[16,17,24,25,29–35] and mollusks[26,36–38] to date from the tropical Pacific (Supplementary Table S1, Fig. 1). Such marine carbonates record the isotopic composition of oxygen (δ^{18}O), which reflects changes in sea-surface temperature (SST, Supplementary Fig. S8a) as well as the δ^{18}O of seawater (the latter linearly related to sea-surface salinity (SSS, Supplementary Fig. S8b). The isotopic signal is generally dominated by the thermal component, except in

the far western Pacific (Supplementary Fig. S9). All records have annual or finer resolution and collectively cover $\sim$ 2000 out of the past 10,000 years (Supplementary Table S1 and Fig. S1). There are three clusters of sites in the western (WP: Papua New Guinea, New Caledonia, Vanuatu, Surprise Atoll), central (CP: the Line Islands of Palmyra, Christmas and Fanning) and eastern (EP: Peruvian coast) tropical Pacific.

The seasonal and interannual components of the tropical Pacific records display much irregularity in interannual (2–7y) variance – a measure of ENSO activity – as well as in the amplitude of the annual cycle (AC). To enable comparisons between different records and sites, we show the ratio between fossil and modern (twentieth century) values of interannual variance and AC amplitude (Fig. 2), with uncertainties estimated via a block bootstrap approach (Supplementary Information). Most records of ENSO variance plot below unity, implying that twentieth century ENSO was unusually active[25]. Those fossil samples displaying higher-than-modern ENSO variance have large uncertainties that are compatible with no change. Such uncertainties are usually the consequence of short modern calibrations.

Despite appreciable differences between ENSO reconstructions from the three regions, some consistent patterns do emerge. In the western Pacific (Fig. 2a), the records show a significant decrease in ENSO variance during the early and mid-Holocene[16,17,30,37]; there are only a few records from the 6-2 kyBP interval but these also show reduced ENSO variance. A decrease in ENSO variance is present throughout the past 7ky in the CP (Fig. 2b), with the most consistent signal corresponding to a 64% reduction in ENSO variance occurring between 3-5 kyBP (Table 1) and a

trend from extremely low variance to the present state from 2 kyBP onwards[24,25]. There are only a few records from the eastern Pacific but these records generally represent longer time spans[26]. They show ENSO variance either similar to or less than today, with the deepest reduction around 4.6 kyBP. Thus, our data set suggests that the mid-Holocene reduction in ENSO identified in previous studies[16–18,33] is not an exceptional event, but rather that ENSO may have been less active than at present for much of the Holocene.

Reconstructions of the AC amplitude calculated for each region are associated with larger uncertainties, and display little coherence through time. Records from the western Pacific show AC amplitudes similar to present before 7 kyBP. However, records from the interval 7-4 kyBP show reduced AC amplitude with low uncertainty, while after 3 kyBP the records show a return to AC amplitudes similar to the present day. In contrast, records from the CP show considerable temporal structure in AC amplitude, although many of the individual records have high levels of uncertainty. In the eastern Pacific, the records show slightly reduced AC amplitude throughout the past 10 ky, except for a period with amplitude similar to the present day at 3 kyBP.

We now use this dataset to constrain the behavior of PMIP3 models. Although there are comparatively few records from precisely 6 kyBP, we assume that the changes recorded during the window between ca 7.5 and 5.5 kyBP are representative of the mid-Holocene and provide an indication of the average change to be expected in the MH simulations. In order to make quantitative model-data comparisons, we translate model output into oxygen isotope ratios using a forward modeling approach[10], in which the $\delta^{18}\mathrm{O}$ of biocarbonates is parameterized as a function of

SSS and SST (Supplementary Information). This provides a record of the isotopic variations that would have been recorded by the coral or mollusk in response to the simulated changes in climate produced by each climate model, which can then be directly compared to the observed variations at a site. The forward model is a simplified representation of the incorporation of $^{18}\mathrm{O}$ by mollusk and coral systems, in particular because it represents the relationship between seawater $^{18}\mathrm{O}$ and SSS as time-invariant (Supplementary Information). However, it has been shown to reproduce the first-order basin-scale variability contained in modern corals from across the tropical Pacific[10]. Thus, since water isotopes are only explicitly modeled in a few GCMs, this simple model provides a way of bridging GCMs and paleo observations.

Most of our records are comparatively short: the average record length is around 50 years (Fig S1b) and very few are longer than 100 years. As ENSO variability is non-stationary, quantifying ENSO variance over such short windows leads to a wide range of estimates[27]. Random sampling of multi-century model simulations under stationary boundary conditions show that ENSO variance estimates on 50-year windows may vary by up to $\pm 50\%$ from sampling alone (Supplementary Figs. S12–S20); these estimates converge as the observation window lengthens. Thus, the short length of most of the observations could make it difficult to discriminate between observed and simulated variability. Changes in the AC amplitude are even more difficult to constrain, but less sensitive to segment length (Supplementary Figs. S11, S12).

We estimate the statistical distributions of modeled ENSO and AC amplitude for 50-year periods via random (block bootstrap) sampling for each model for the piControl and midHolocene

simulations (Supplementary Table S2) and compare these distributions to the values obtained from the Historical simulations (Supplementary Fig. S12-19). The distributions of both ratios are broad and positively skewed (Supplementary Fig. 2, colored curves). ENSO variance ratios are clustered around unity in the piControl experiments, and fall below unity in most of the midHolocene experiments. The midHolocene reduction is small and, given the width of the distributions, only marginally significant at the 5% level. Nonetheless, it is qualitatively consistent with results from an intermediate complexity model[2] as well as many other GCM simulations[4,5,8,11], all of which show reduced ENSO variability during the mid-Holocene compared to the pre-industrial climate.

While the synthesis of existing paleo-ENSO data present a heterogeneous picture of ENSO variability through both space and time, there is evidence for a sustained reduction in ENSO variability from 3-5 kyBP. This is especially true in the CP, where a deep reduction (64%) is accompanied by a relatively narrow 95% confidence interval (CI) of $[28\%, 84\%]$ (Table 1). Reductions of similar magnitude are observed during the MH (5.5-7.5 kyBP) (66% in the center, 50% in the West, 33% in the East), albeit with CIs so wide that they cannot exclude increases in ENSO variance (Table 1). Thus, a salient feature of this dataset is a robust, approximately two-thirds reduction in CP interannual variance, which seems to have persisted throughout much of the 3-5 kyBP interval. This persistent reduction bears little resemblance to the response expected from insolation forcing alone[2,15], and happened at a time when boreal summer/winter precessional forcing is weaker than during the MH (Supplementary Fig. S7). Can PMIP3 GCMs simulate such reductions, and if so, under which conditions? We answer this question by computing the probability of observing ENSO variance reductions of at least 64% on 50-year segments (Table 2). These probabilities are

extremely low under pre-industrial conditions, ranging from 0.58 to 12.15%. Such occurrences are still rare under MH boundary conditions (probabilities ranging from 0.42 to 16.20%), though most (7 out of 9) of the models show an increased probability of ENSO reduction. Thus, while orbital forcing characteristic of the MH tends to drive simulated changes in ENSO variance in the right direction, the amplitude of simulated changes is too modest, and the response is not consistent among all models. It is even harder to explain even larger, more sustained reductions that may have prevailed during the 3-5 kyBP period, but the short length of the simulations, either forced or unforced (Supplementary Table S2), precludes an assessment of this question.

The models all show a reduction in the median amplitude of the AC in the midHolocene simulations, for all three regions. The reduction is between 10% to 40% (depending on the model) but is relatively uniform across the basin (Fig. 2, right). This uniformity contrasts strongly with the observed changes in the 7.5-5.5 kyBP window, where AC amplitude is decreased in the western Pacific but increased in the CP. However, the reduction in AC amplitude in the western Pacific is $\sim 50\%$ larger than in the simulations.

We investigate the link between changes in ENSO variance and in AC amplitude by plotting the fossil to modern ratio of ENSO-band variance against the same ratio of AC amplitude, in both observations and GCMs (Fig. 3). Both axes are scaled by their uncertainty to make an orthogonal regression possible (Methods). Despite uncertainties, we find a significant positive relationship between ENSO variance and AC amplitude in the observations (Fig. 3, top). However, the simulated relationship is negative (Fig. 3, bottom), in agreement with previous work[3,6,13,39], but only

marginally significant. Moreover, the range of variations in AC amplitude is about 7 times larger in the observations than in the simulations (Supplementary Fig. S21). Similar results emerge if only data from the CP are considered (Supplementary Figs. S22–23), or if wavelet analysis is used to diagnose the relationship between energy in the annual and interannual bands[39] (Supplementary Fig. S24). If our interpretation of the data is correct, the mismatch between the observed and simulated relationship between ENSO variance and AC amplitude has important dynamical implications. The frequency entrainment hypothesis[3,12] has long been invoked to explain the inverse relationship between ENSO and the AC in coupled GCMs [5,6,11,13]. Our results suggest that this link is relatively weak in models, and opposite to that found in observations over the Holocene.

In comparing the ENSO-AC relationship across models and data, it is important to note the limitations associated with using a sparse set of observations to represent tropical Pacific dynamics. One possible explanation is that uncertainties in AC amplitude estimates from corals are more uncertain than depicted by the bootstrap intervals, as documented by discrepancies of up to 30% in AC estimates from overlapping coral δ^{18}O records from the central tropical Pacific (Supplementary Fig. S11). The relationship between δ^{18}O and SSS is poorly constrained on subannual scales, and may vary across a given reef environment, further confounding estimates of AC amplitude changes from high-resolution archives. Results are, however, insensitive to the choice of ENSO metric as long as fossil/modern ratios are used (Supplementary Fig. S26).

Changes in the spatial characteristics of ENSO represent another source of uncertainty, as different flavors of ENSO have different impacts on SST and SSS across the study domain[40].

Canonical El Niño events involve temperature changes in the eastern Pacific (EP). However, many events peak in the CP[41]. Indeed, changes in the prevalence of ENSO flavors in the Holocene have been suggested by changes in the asymmetry of ENSO anomalies in the eastern Pacific[26] as well as analysis of PMIP3 midHolocene simulations[11,42]. Thus, some of the observed variations in ENSO intensity/frequency over the Holocene could reflect changes in the spatial pattern of ENSO and differences between individual records could reflect a dominance of one expression of ENSO over another[26]. Note, however, that a simple ENSO model suggests that modern changes in the prevalence of ENSO flavors may arise internally[43]. Our dataset is too sparse to resolve spatial features of ENSO or the AC structure, but it is hoped that denser observational networks will shed light on these questions in the future.

It has been suggested that boreal fall insolation, which peaks at $\sim$5 kyBP (Supplementary Fig. S7), modulates ENSO variability via air/sea coupling strength[2]. However, our analyses reveal that changes in ENSO variance and AC amplitude over the Holocene bear no simple relation to orbital forcing, excluding a linear mechanism. It is possible that millennial-scale changes in ENSO variability arose either (1) internally, (2) as a non-linear response to orbital forcing, or (3) result from other factors, such as the presence of a remnant Laurentide ice sheet, that modulated the response to orbital forcing[9]. This set of observations suggests persistent changes in ENSO variance and AC amplitude that fall well outside the range shown by both pre-industrial and midHolocene PMIP3 simulations, particularly during the 3-5 kyBP interval. This indicates that this set of climate models does not capture the potential range of ENSO variability, and suggests a new target for climate models of varying complexity to reproduce and explain. One challenge in simulat-

ing such changes with GCMs is that computational requirements typically restrict simulations to 100-200yrs, on average. As computational power increases, long transient runs, both forced[5] and unforced[27], will be essential to distinguish endogenous from exogenous sources of variability in ENSO. Furthermore, the observed relationship between ENSO variance and AC amplitude is opposite to that simulated by most PMIP3 GCMs – though both datasets are statistically compatible with a lack of relationship. GCMs where this relationship dominates the ENSO response to orbital forcing may therefore not be representative of the real world.

While precessional and greenhouse gas forcing are fundamentally different in character, our work demonstrates the ability of high-resolution paleoclimate records to provide fundamental constraints on tropical climate dynamics, as represented in models used to project twenty-first century climate trends. In that context, the fact that ENSO seems relatively impervious to external forcing suggests that its future evolution may be chiefly governed by internal processes, placing fundamental limits on its long-term predictability. Understanding internal processes of low-frequency ENSO modulation, and the extent to which they are captured by climate models, is therefore of utmost importance to climate prediction.

Methods

Multi-proxy synthesis Changes in ENSO variance ratios were quantified by computing the ratio of fossil to modern variance in the 2-7y band, isolated via a (Morlet) wavelet filter (results are not sensitive to the filter type). AC amplitude was quantified as the largest seasonal range experienced

by each proxy over its time span. Changes in this quantity were, as in ENSO variance, computed as the ratio between fossil and modern samples. Uncertainties in both quantities were estimated via a block-bootstrap procedure [44,45] with $N = 1,000$ draws. For interannual variance, the block length was set at 2 years, while for seasonal amplitude the block length was set at 1 year. Both choices reflect a tension between the approximate decorrelation time of the records for their respective signals and the shortness of some proxy records.

Analysis of GCM simulations GCM-simulated SST and SSS were translated to coral δ^{18}Ovalues a forward model[10]. Those pseudocoral fields for the three main regions (WP, CP, EP) were then resampled using the above-mentioned block-boostrap procedure with $N = 1,000$ draws, before being subsampled on contiguous 50-year blocks to emulate short observational windows. We then computed ENSO variance and AC amplitude, as well as their ratios, for each ensemble member. Probability distributions from these 1,000 member ensembles were then obtained via kernel density estimation with a bandwidth $h = 0.15$.

Regression Analysis We use total least squares (TLS) regression (a form of error-in-variables modeling, closely connect to orthogonal regression[46]), to account for uncertainties in the ENSO - AC amplitude relationship. TLS steepens regression slopes in taking the potentially biasing effects of observational noise into account[47]. ENSO variance and AC amplitude ratios were scaled by their uncertainty (measured by the interquartile range of their block-bootstrap distributions) prior to TLS regression, to ensure homogenous error magnitudes on both axes of Fig 3.

Wavelet Analysis The relationship between ENSO and the AC is also probed via Morlet wavelet analysis[48]. We sum the energies corresponding to the 2-7y and 0.8-1.2 y bands and report linear correlations between the resulting series[39]. Statistical significance is established via a non-parametric, isospectral test[49].

Data The proxy data synthesis is available for download from NOAA National Climatic Data Centre Paleoclimatology database (`http://www.ncdc.noaa.gov/paleo/paleo.html`) at the following URL [placeholder]. The model data is available via the CMIP5/PMIP3 (`http://cmip-pcmdi.llnl.gov/cmip5/`) web site.

Bibliography

1. Collins, M. *et al.* The impact of global warming on the tropical Pacific Ocean and El Niño. *Nature Geosci* **3**, 391–397 (2010).

2. Clement, A. C., Seager, R. & Cane, M. A. Suppression of El Niño during the mid-Holocene by changes in the Earth's orbit. *Paleoceanography* **15**, 731–737 (2000).

3. Liu, Z. A Simple Model Study of ENSO Suppression by External Periodic Forcing. *Journal of Climate* **15**, 1088–1098 (2002).

4. Zheng, W., Braconnot, P., Guilyardi, E., Merkel, U. & Yu, Y. ENSO at 6ka and 21ka from ocean–atmosphere coupled model simulations. *Clim. Dyn.* **30**, 745–762 (2008).

5. Liu, Z. *et al.* Evolution and forcing mechanisms of El Nino over the past 21,000 years. *Nature* **515**, 550–553 (2014).

6. Timmermann, A., Lorenz, S. J., An, S.-I., Clement, A. & Xie, S.-P. The effect of orbital forcing on the mean climate and variability of the tropical pacific. *Journal of Climate* **20**, 4147–4159 (2007).

7. Timmermann, A. *et al.* The Influence of a Weakening of the Atlantic Meridional Overturning Circulation on ENSO. *Journal of Climate* **20**, 4899–4919 (2007).

8. Chiang, J. C. H., Fang, Y. & Chang, P. Pacific Climate Change and ENSO Activity in the Mid-Holocene. *Journal of Climate* **22**, 923–939 (2009).

9. Luan, Y., Braconnot, P., Yu, Y. & Zheng, W. Tropical pacific mean state and enso changes: sensitivity to freshwater flux and remnant ice sheets at 9.5 ka bp. *Climate Dynamics* **44**, 661–678 (2015).

10. Thompson, D. M., Ault, T. R., Evans, M. N., Cole, J. E. & Emile-Geay, J. Comparison of observed and simulated tropical climate trends using a forward model of coral $\delta^{18}\mathrm{O}$. *Geophys. Res. Lett.* **38** (2011).

11. An, S.-I. & Choi, J. Mid-Holocene tropical Pacific climate state, annual cycle, and ENSO in PMIP2 and PMIP3. *Climate Dynamics* **43**, 957–970 (2014).

12. Chang, P., Wang, B., Li, T. & Ji, L. Interactions between the seasonal cycle and the Southern Oscillation - Frequency entrainment and chaos in a coupled ocean-atmosphere model. *Geophys. Res. Lett.* **21**, 2817–2820 (1994).

13. An, S.-I. *et al.* The Inverse Effect of Annual-Mean State and Annual-Cycle Changes on ENSO. *Journal of Climate* **23**, 1095–1110 (2010).

14. Schmidt, G. A. Enhancing the relevance of palaeoclimate model/data comparisons for assessments of future climate change. *Journal of Quaternary Science* **25**, 79–87 (2010).

15. Braconnot, P., Luan, Y., Brewer, S. & Zheng, W. Impact of Earth's orbit and freshwater fluxes on Holocene climate mean seasonal cycle and ENSO characteristics. *Climate Dynamics* **38**, 1081–1092 (2012).

16. Tudhope, A. W. *et al.* Variability in the El Niño- Southern Oscillation Through a Glacial-Interglacial Cycle. *Science* **291**, 1511–1517 (2001).

17. McGregor, H. V. & Gagan, M. K. Western Pacific coral δ^{18}O records of anomalous Holocene variability in the El Niño-Southern Oscillation. *Geophysical Research Letters* **31** (2004).

18. Koutavas, A. & Joanides, S. El Niño-Southern Oscillationextrema in the Holocene and Last Glacial Maximum. *Paleoceanography* **27**, PA4208 (2012).

19. Wang, X. L. The Coupling of the Annual Cycle and ENSO Over the Tropical Pacific. *Journal of the Atmospheric Sciences* **51**, 1115–1136 (1994).

20. Guilyardi, E. El Niño mean state seasonal cycle interactions in a multi-model ensemble. *Clim. Dyn.* **26**, 329–348 (2006).

21. Tziperman, E., Stone, L., Cane, M. A. & Jarosh, H. El Niño Chaos: Overlapping of Resonances Between the Seasonal Cycle and the Pacific Ocean-Atmosphere Oscillator. *Science* **264**, 72–74 (1994).

22. Jin, F.-F., Neelin, J. D. & Ghil, M. El Niño on the Devil's Staircase: Annual Subharmonic Steps to Chaos. *Science* **264**, 70–72 (1994).

23. Stuecker, M. F., Timmermann, A., Jin, F.-F., McGregor, S. & Ren, H.-L. A combination mode of the annual cycle and the El Niño-Southern Oscillation. *Nature Geosci* **6**, 540–544 (2013).

24. McGregor, H. V. *et al.* A weak El Niño-Southern Oscillationwith delayed seasonal growth around 4,300 years ago. *Nature Geoscience* **6**, 949–953 (2013).

25. Cobb, K. M. *et al.* Highly Variable El Niño-Southern OscillationThroughout the Holocene. *Science* **339**, 67–70 (2013).

26. Carré, M. *et al.* Holocene history of ENSO variance and asymmetry in the eastern tropical Pacific. *Science* **345**, 1045–1048 (2014).

27. Wittenberg, A. T. Are historical records sufficient to constrain ENSO simulations? *Geophys. Res. Lett.* **36** (2009).

28. Braconnot, P. *et al.* Evaluation of climate models using palaeoclimatic data. *Nature Clim. Change* **2**, 417–424 (2012).

29. Cobb, K. M., Charles, C. D., Cheng, H. & Edwards, R. L. El Niño/Southern Oscillation and tropical Pacific climate during the last millennium. *Nature* **424**, 271–276 (2003).

30. Duprey, N. *et al.* Early mid-Holocene SST variability and surface-ocean water balance in the southwest Pacific. *Paleoceanography* **27**, 4207 (2012).

31. Kilbourne, K. H., Quinn, T. M., Taylor, F. W., Delcroix, T. & Gouriou, Y. El Niño-Southern Oscillation-related salinity variations recorded in the skeletal geochemistry of a Porites coral from Espiritu Santo, Vanuatu. *Paleoceanography* **19**, 4002–+ (2004).

32. Woodroffe, C. D. & Gagan, M. K. Coral microatolls from the central Pacific record Late Holocene El Niño. *Geophysical Research Letters* **27**, 1511–1514 (2000).

33. Woodroffe, C. D., Beech, M. R. & Gagan, M. K. Mid-late Holocene El Niño variability in the equatorial Pacific from coral microatolls. *Geophysical Research Letters* **30**, 1358 (2003).

34. Evans, M., Fairbanks, R. & Rubenstone, J. A proxy index of ENSO teleconnections. *Nature* **394**, 732–733 (1998).

35. McGregor, H. V., Fischer, M. J., Gagan, M. K., Fink, D. & Woodroffe, C. D. Environmental control of the oxygen isotope composition of porites coral microatolls. *Geochimica et Cosmochimica Acta* **75**, 3930–3944 (2011).

36. Carré, M., Sachs, J. P., Schauer, A. J., Rodríguez, W. E. & Ramos, F. C. Reconstructing El Niño - Southern Oscillation activity and ocean temperature seasonality from short-lived marine mollusk shells from Peru. *Palaeogeography, Palaeoclimatology, Palaeoecology* **371**, 45–53 (2013).

37. Driscoll, R. *et al.* ENSO Reconstructions over the past 60 ka using giant clams (Tridacna sp.) from Papua New Guinea. *Geophysical Research Letters* 2014GL061446 (2014).

38. Welsh, K., Elliot, M., Tudhope, A., Ayling, B. & Chappell, J. Giant bivalves (Tridacna gigas) as recorders of ENSO variability. *Earth and Planetary Science Letters* **307**, 266–270 (2011).

39. An, S.-I. & Choi, J. Inverse relationship between the equatorial eastern Pacific annual-cycle and ENSO amplitudes in a coupled general circulation model. *Climate Dynamics* **40**, 663–675 (2013).

40. Kug, J.-S., Jin, F.-F. & An, S.-I. Two types of El Niño events: Cold tongue El Niño and warm pool El Niño. *Journal of Climate* **22**, 1499–1515 (2009).

41. Trenberth, K. E. & Stepaniak, D. P. Indices of El Niño Evolution. *Journal of Climate* **14**, 1697–1701 (2001).

42. Karamperidou, C., Di Nezio, P. N., Timmermann, A., Jin, F.-F. & Cobb, K. M. The response of ENSO flavors to mid-Holocene climate: Implications for proxy interpretation. *Paleoceanography* 2014PA002742 (2015). URL `http://dx.doi.org/10.1002/2014PA002742`.

43. Newman, M., Shin, S.-I. & Alexander, M. A. Natural variation in ENSO flavors. *Geophys. Res. Lett.* **38** (2011).

44. Efron, B. & Tibshirani, R. J. *An Introduction to the Bootstrap* (Chapman & Hall, New York, 1993).

45. Kunsch, H. R. The Jackknife and the Bootstrap for General Stationary Observations. *The Annals of Statistics* **17**, 1217–1241 (1989). URL `http://dx.doi.org/10.2307/2241719`.

46. Van Huffel, S. *Total Least Squares and Errors- In-Variables Modeling: Bridging the Gap Between Statistics, Computational Mathematics and Engineering*, 539–555 (Physica-Verlag HD, 2004). URL http://dx.doi.org/10.1007/978-3-7908-2656-2_44.

47. Markovsky, I., Sima, D. M. & Van Huffel, S. Total least squares methods. *Wiley Interdisciplinary Reviews: Computational Statistics* **2**, 212–217 (2010). URL http://dx.doi.org/10.1002/wics.65.

48. Torrence, C. & Compo, G. P. A practical guide to wavelet analysis. *Bull. Amer. Meteor. Soc.* **79**, 61–78 (1998).

49. Ebisuzaki, W. A method to estimate the statistical significance of a correlation when the data are serially correlated. *Journal of Climate* **10**, 2147–2153 (1997).

Supplementary Information is linked to the online version of the paper at www.nature.com/ngeo.

Acknowledgements

We proactively thank the referees for constructive reviews that will improve the manuscript. All data, metadata and code [will be] archived at NCDC (URL placeholder). We acknowledge the World Climate Research Program's Working Group on Coupled Modelling, which is responsible for CMIP, and we thank the PMIP3 modeling groups for producing and making available their model output. The U.S. Department of Energy's Program for Climate Model Diagnosis and Inter-

comparison provides coordinating support for CMIP, and led development of software infrastructure in partnership with the Global Organization for Earth System Science Portals. JEG acknowledges support from US NSF grant DMS 1025465. KMC acknowledges support from NOAA award NA11OAR4310166 and NSF award OCE-0752091. M. Collins acknowledges support from UK NERC grant NE/H009957/1. HVM and AT acknowledge support from Australian Research Council (ARC) Discovery Project grant DP1092945. HVM is supported by an ARC Future Fellowship FT140100286 grant. AT acknowledges support from UK NERC grant NE/H009957/1. TC thanks M. McCulloch (formerly at ANU) for dating the Bayes coral, and M. Gagan's team at ANU for help with isotopic measurements. The Bayes 1 core was collected with funds from the Institut de Recherche pour le Développement. BS was supported by the DFG Cluster of Excellence "The Future Ocean" (EXC 80/2). PB, M. Carré, TC, JL, ME and AT were supported by the French National Research Agency under EL PASO grant (no. 2010 298 BLANC 608 01). This project also serves for coordination and implementation of the PMIP3/CMIP5 simulations on the ESGF distributed database. We thank Jean-Yves Peterschmitt for his help with the PMIP database. This work was initiated in a workshop co-sponsored by WCRP/CLIVAR, IGBP/PAGES, INQUA, and IPSL in 2011.

Author Contributions

J.E.G. designed the study, performed the analysis, lead the writing, and prepared the manuscript. P.B. coordinated the synthesis. M.Carré, KMC, T.C., M.E. and R.D. contributed data and/or analysis. P.B. and J.L. analyzed simulations and contributed to writing. Y.Z. processed PMIP3 output

and prepared some of the supplementary figures. A.T., B.S., M.Collins provided input in the analysis and interpretation. J.E.G., K.M.C., S.P.H., H.V.M., T.C., P.B. and A.T. wrote the paper. All authors reviewed the manuscript.

Author information

Reprints and permissions information is available at `www.nature.com/reprints`. The authors declare no competing financial interests. Correspondence and requests for materials should be addressed to julieneg@usc.edu.

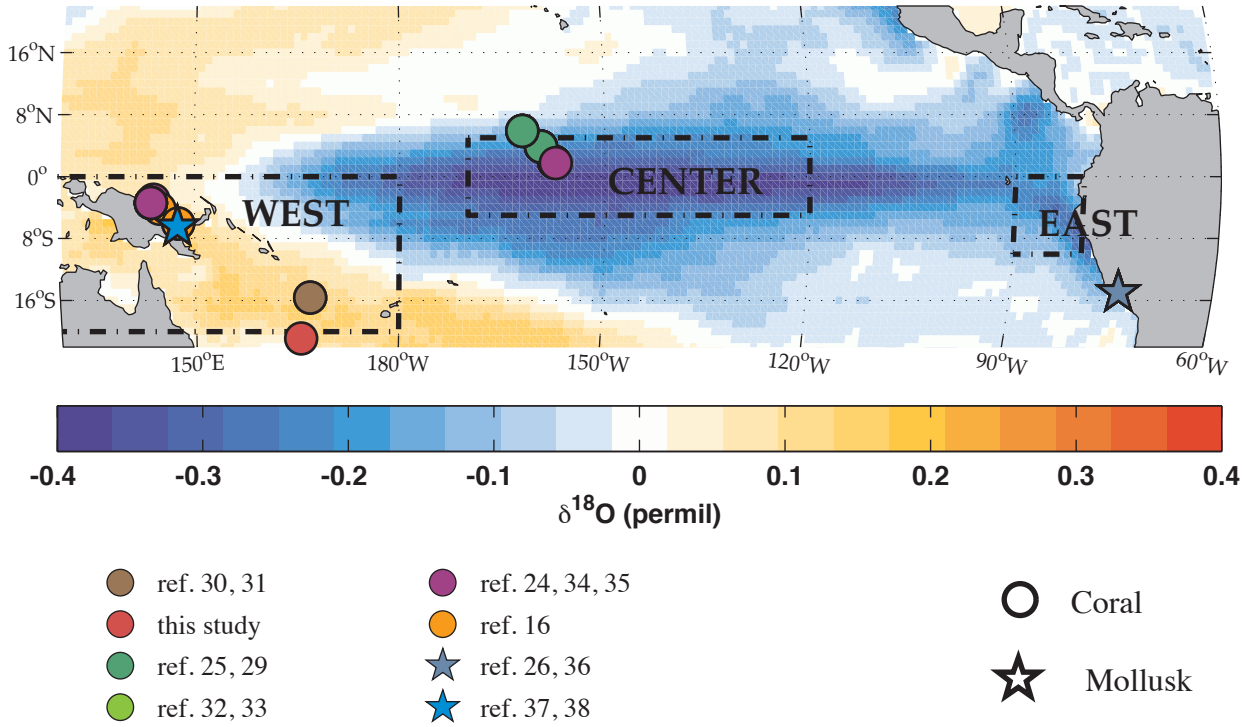

Figure 1: Location and ENSO sensitivity of proxy archives. Circles denote corals, stars denote mollusks. Contours denote biocarbonate δ^{18}O composites (per °C of NINO3.4 SST) derived from the model of Thompson et al. [10] driven by NCEP OI analysis v2 SST and SODA 2.2.4 SSS over 1981-2010 boreal winters (Supplementary Fig. S8-S9). δ^{18}O values were regressed onto NINO3.4 SST to highlight relationships to ENSO. The three equatorial study regions (West, Center & East) are delineated by boxes.

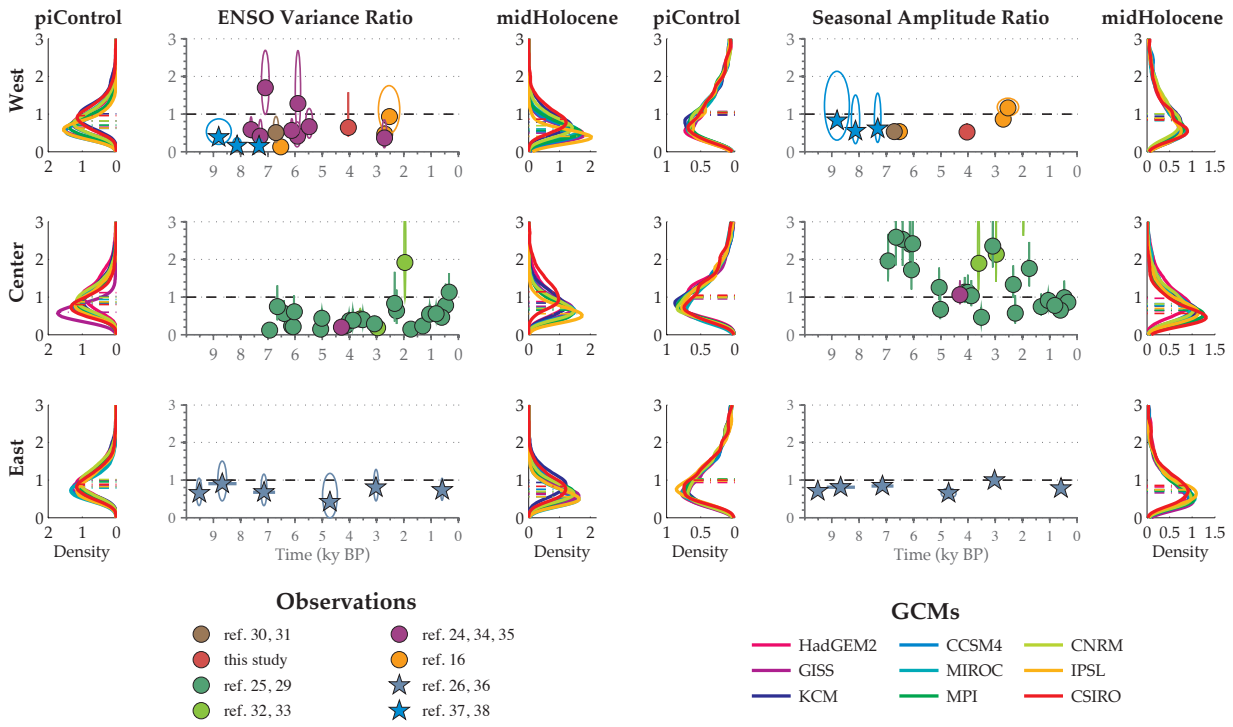

Figure 2: (top) Changes in seasonal and interannual variance over the Holocene. LEFT column: Changes in ENSO-band (2-7y) variance between fossil and modern samples for the three study regions, West (top), Center (middle) and East (bottom). Horizontals bars span the period covered by each dataset; except for mollusks from the Peruvian coast, these bars are usually narrower than the symbol width. Ellipses represent uncertainties about these ratios in both dimensions: the width of each ellipse represents a 95% confidence interval for the central date of each sample, based on reported analytical uncertainty on radiometric ages; the vertical component of each ellipse represents a 95% confidence interval for the variance ratio, obtained via a block-bootstrap procedure (Methods). Unity (no change) is marked by a dashed gray line. Similar statistics derived from PMIP3 models on 50-year windows are depicted on side panels for piControl and MidHolocene experiments. RIGHT column: idem for seasonal amplitude (Methods).

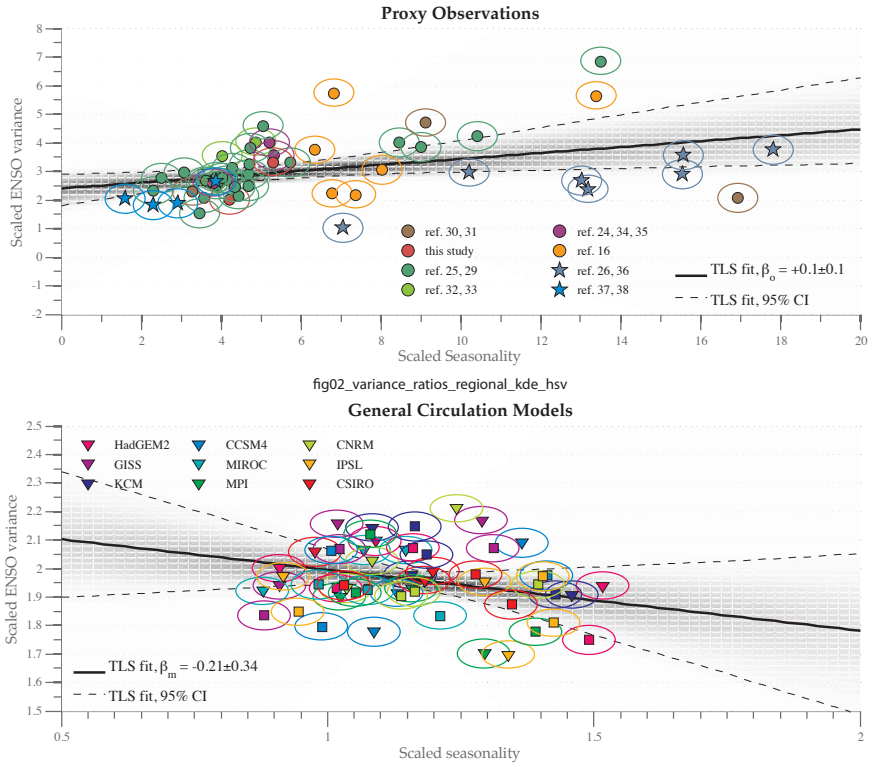

Figure 3: (top) Link between ENSO variance and the seasonal cycle in proxy observations (top) and PMIP3 models (bottom). The observed values are for all seasonally-resolved records from the Pacific during the whole of the past 10 ky. The simulated values are based on 50-year segments from the midHolocene and piControl simulations. On top, symbology as in Fig 1. On the bottom, triangles denote the median of piControl simulations, squares the median of midHolocene simulations. Data from the eastern, central and western Pacific were pooled together, scaled by their interquartile range so their uncertainties on both axes are commensurate. An orthogonal regression (total least squares) fit is presented for both datasets, together with approximate 95% confidence intervals (dashed lines) and probability density (gray contours) obtained via bootstrap resampling (Methods).

		Quantiles		
Period	**Region**	2.5%	50%	97.5%
5.5 – 7.5 kyBP	West	-125%	50%	92%
	Center	-5%	66%	92%
	East	-16%	33%	69%
3–5 kyBP	West	-54%	35%	61%
	Center	28%	64%	84%
	East	-18%	58%	109%

Table 1: Observed reductions in ENSO variance in the tropical Pacific during the MH (5.5–7.5 kyBP) and the 3-5 kyBP interval. The numbers represent quantiles of the block-bootstrap ensembles. By convention, a negative reduction implies an increase.

H_0	HadGEM2	GISS	KCM	CCSM4	MIROC	MPI	CNRM	IPSL	CSIRO
PI null	0.58%	12.15%	1.42%	3.33%	1.53%	3.87%	1.15%	2.52%	3.66%
MH null	2.87%	4.61%	3.68%	5.15%	8.20%	11.49%	6.50%	16.20%	0.42%

Table 2: Probability of observing periods of reduced ENSO activity in the CP in nine GCMs. Top row: frequency of occurrence of 50-year long periods for which the ENSO variance ratio is as low as the 3-5 kyBP average inferred from paleoclimate observations (0.36 – a 64% reduction) in pre-industrial (piControl) simulations. Bottom row: same for midHolocene simulations